10-1-2020

Land Use and Season Influence Event-Scale Nitrate and Soluble Reactive Phosphorus Exports and Export Stoichiometry from Headwater Catchments

Dustin W. Kincaid
University of Vermont

Erin C. Seybold
University of Vermont

E. Carol Adair
University of Vermont

William B. Bowden
University of Vermont

Julia N. Perdrial
University of Vermont

See next page for additional authors

Recommended Citation

Kincaid DW, Seybold EC, Adair EC, Bowden WB, Perdrial JN, Vaughan MC, Schroth AW. Land Use and Season Influence Event-Scale Nitrate and Soluble Reactive Phosphorus Exports and Export Stoichiometry from Headwater Catchments. Water Resources Research. 2020 Oct;56(10):e2020WR027361.

AGU ADVANCING EARTH AND SPACE SCIENCE

Water Resources Research

RESEARCH ARTICLE
10.1029/2020WR027361

Land Use and Season Influence Event-Scale Nitrate and Soluble Reactive Phosphorus Exports and Export Stoichiometry from Headwater Catchments

Dustin W. Kincaid[1], Erin C. Seybold[1,2], E. Carol Adair[1], William B. Bowden[1], Julia N. Perdrial[1], Matthew C. H. Vaughan[3], and Andrew W. Schroth[1]

[1]University of Vermont, Burlington, VT, USA, [2]Kansas Geological Survey, University of Kansas, Lawrence, KS, USA, [3]Lake Champlain Basin Program, Grand Isle, VT, USA

Key Points:
- High-frequency sensors revealed C-Q patterns that provide valuable information on source areas and transport pathways for nitrate and SRP
- Source and transport pathways differed for nitrate and SRP and were influenced by land use/land cover and seasonal dynamics
- Seasonal patterns in event nitrate to SRP ratios were similar among sites, but were driven by site-specific nitrate and SRP export dynamics

Supporting Information:
- Supporting Information S1

Correspondence to:
D. W. Kincaid,
dustinkincaid@gmail.com

Citation:
Kincaid, D. W., Seybold, E. C., Adair, E. C., Bowden, W. B., Perdrial, J. N., Vaughan, M. C. H., & Schroth, A. W. (2020). Land use and season influence event-scale nitrate and soluble reactive phosphorus exports and export stoichiometry from headwater catchments. *Water Resources Research*, *56*, e2020WR027361. https://doi.org/10.1029/2020WR027361

Received 17 FEB 2020
Accepted 18 SEP 2020
Accepted article online 23 SEP 2020

Abstract Catchment nutrient export, especially during high flow events, can influence ecological processes in receiving waters by altering nitrogen (N) and phosphorus (P) concentrations and relative amounts (stoichiometry). Event-scale N and P export dynamics may be significantly altered by land use/land cover (LULC) and season. Consequently, to manage water resources, it is important to understand how LULC and season interact to influence event N and P export. In situ, high-frequency spectrophotometers allowed us to continuously and concurrently monitor nitrate (NO_3^-) and soluble reactive P (SRP) concentrations and therefore examine event-scale NO_3^- and SRP export dynamics. Here we analyzed event NO_3^- and SRP concentration-discharge hysteresis patterns and yields for >400 events to evaluate how LULC and seasonality influence event NO_3^- and SRP export dynamics in three low-order watersheds with different primary LULCs (agricultural, forested, and urban). Differences among event NO_3^- and SRP hysteresis patterns suggest these nutrients have different source areas and dominant transport pathways that were impacted by both LULC and seasonality. Unexpectedly, we observed similar seasonal patterns in event NO_3^-:SRP stoichiometry among LULCs, with the most N-enriched events occurring in spring, and event stoichiometry approaching Redfield N:P ratios in the fall. However, seasonal stoichiometry patterns were driven by unique seasonal NO_3^- and SRP export patterns at each site. Overall these findings suggest LULC and seasonality interact to alter the timing and magnitude of event NO_3^- and SRP exports, leading to seasonal patterns in event NO_3^- to SRP stoichiometry that may influence ecological processes, such as productivity, in receiving waters.

Plain Language Summary High flow events transport relatively large quantities of nitrogen (N) and phosphorus (P) to streams and downstream waterbodies where they may stimulate algal blooms and degrade water quality. We evaluated how land uses and seasons alter event nutrient transport. We monitored >400 events with sensors in streams with contrasting land uses. Event N and P concentration patterns differed from each other suggesting dissolved N and P were transported from different locations in the landscape. Further, the agricultural and urban streams received more dissolved N and P than the forested stream. This likely results from fertilizer applications in excess of crop (agricultural and lawn grass) needs and landscape modifications, such as drainage systems and impervious surfaces, that limit soils and vegetation from removing nutrients from runoff. Lastly, season influenced the ratio of dissolved N to P delivery, with spring events transporting the most N relative to P and fall events transporting the least. Overall, land use and season uniquely influenced event nutrient transport. Management strategies to reduce algal blooms in downstream waterbodies must consider interactions among land use, nutrient type, and season. However, ratios of N to P may change seasonally but independently of land use, which could simplify management approaches.

1. Introduction

High flow events, such as those driven by snowmelt and rain events, are important drivers of dissolved nutrient transport from terrestrial landscapes to stream networks (Dhillon & Inamdar, 2013; Frazar et al., 2019; Inamdar et al., 2006; Janke et al., 2013; Perdrial et al., 2014; Rosenberg & Schroth, 2017; Sharpley et al., 2008). Nutrient transport to stream networks can impact ecological processes in receiving waters by altering absolute nutrient concentrations and the relative availability, or stoichiometric ratios,

of nutrients (Isles et al., 2017). The stoichiometric ratio of nitrogen (N) to phosphorus (P) can influence a range of ecological processes (Frost et al., 2005; Sardans et al., 2011), including phytoplankton community composition (Poxleitner et al., 2016; Tilman et al., 1982), the probability of toxin-producing algal blooms (Davidson et al., 2012; Michalak et al., 2013), and trophic interactions (Elser et al., 2010). Thus, it is essential to understand how high flow events drive dissolved N and P transport dynamics and resulting N:P ratios. Currently, our understanding of how key drivers of nutrient transport differently influence dissolved N and P transport during high flow events is limited (Frazar et al., 2019; Gächter et al., 2004; Gao et al., 2014; Vanni et al., 2001). For example, characterizing how land use/land cover (LULC) and seasons have different effects on factors that influence event N versus P transport dynamics, such as sources, dominant transport pathways, and timing of their activation during events. A better understanding of these differences will improve our ability to control downstream N and P transport and the resulting stoichiometry of nutrients in receiving waters.

Dissolved N and P accumulate in and move through catchments differently as a result of their different affinities for the soil matrix. Nitrate (NO_3^-), a soluble anion with little affinity for the soil matrix, moves relatively freely through catchment soils and often enters streams with groundwater baseflow (Hobbie et al., 2017; Vanni et al., 2001). Conversely, phosphate (PO_4^{3-}), commonly measured as soluble reactive P (SRP), readily adsorbs to soil particles and is much less mobile than NO_3^- (Holtan et al., 1988). Consequently, SRP accumulates in upper soil horizons and is transported to streams in particulate form with eroded soils (Holtan et al., 1988; Ockenden et al., 2016) or as mobile SRP in surface and subsurface flowpaths (Dupas et al., 2015; Stutter et al., 2008). As such, varying hydrologic conditions (e.g., antecedent moisture conditions, event sizes, stream flow, etc.) may activate different source areas and transport pathways, driving differences in the timing and magnitude of NO_3^- versus SRP transport to stream networks.

Seasonally related factors, specifically precipitation and temperature, modify solute transformation rates and transport dynamics and often produce seasonal patterns of NO_3^- and SRP export. During cool and winter months in the northeastern United States (late fall through early spring), biological assimilation, especially vegetation uptake, is limited and NO_3^- accumulates in snowpack and in soils underlying snowpack (Brooks et al., 1998; Campbell et al., 2006). Consequently, early season runoff is enriched with NO_3^-, and the majority of annual NO_3^- export occurs with snowmelt and winter/spring rain runoff (Pellerin et al., 2012; Seybold et al., 2019). However, LULC and management practices (e.g., manure and fertilizer applications) can alter this seasonal pattern by contributing highly concentrated sources to the landscape during subsequent seasons (Seybold et al., 2019; Vaughan et al., 2017). Contrary to NO_3^-, seasonal patterns in stream SRP concentrations are less apparent in northern hardwood forests (Meyer & Likens, 1979), but seasonal SRP concentration reductions can be driven by in-stream biological uptake during periods of maximum heterotrophic and autotrophic activity in more southern forested streams (Mulholland, 2004). Thus, differences in seasonal NO_3^- and SRP export dynamics may cause event N and P stoichiometry to evolve seasonally.

LULC further impacts NO_3^- and SRP transport by altering inputs and transport pathways. Inputs associated with agriculture (e.g., manure and fertilizer) and urbanization (e.g., emissions from fossil fuel combustion, fertilizers, household pet waste, and sanitary sewers) increase the supply of NO_3^- and SRP available for transport in the landscape (Driscoll et al., 2003; Duan et al., 2012; Dubrovsky et al., 2011; Hobbie et al., 2017). Agricultural practices and urbanization also modify landscapes to efficiently route runoff to surface waters and consequently diminish their capacity to process and retain NO_3^- and SRP. For example, artificial drainage systems (e.g., subsurface tile drains) in agricultural fields often bypass nutrient removal hotspots, including wetlands and riparian areas (Royer et al., 2006). Similarly, impervious surfaces and stormwater drainage infrastructure in urbanized areas reduce water residence times and interaction with removal zones in soils and riparian areas (Bernhardt et al., 2008). Together these modifications alter solute exports and transport dynamics (Seybold et al., 2019; Vaughan et al., 2017, 2019).

Ideally, to understand how LULC and seasonality differentially alter event N versus P transport dynamics we would directly measure all potential sources and transport pathways within the landscape and the temporal variability in their activation during events. However, direct measurement of these transport dynamics while desirable would be prohibitively expensive. As an alternative, we can use in situ sensors and novel algorithms to measure nutrient concentrations at high frequencies and quantify concentration-discharge

Table 1
Study Area Characteristics

	Hungerford Brook	Potash Brook	Wade Brook
Primary land cover	Agricultural	Urban	Forested
Catchment area (km^2)	48.1	18.4	16.7
Forested area (%)	40.5	10.6	95.1
Agricultural area (%)	44.8	29.1	0.6
Urban area (%)	5.6	53.5	0.8
Impervious area (%)	2.3	23.9	0.0
Wetland area (%)	21.5	12.4	1.9
Sensor elevation (m)	80	42	320
Maximum catchment elevation (m)	354	143	981
Mean catchment slope (%)	5.6	5.3	26
Mean air temperature (°C)	6.7	7.8	4.2
Mean precipitation (mm yr^{-1})	1,000	961	1,453
Mean annual atmospheric nitrogen deposition (kg N km^{-2})	450	340	570
Sensor optical path length used (mm)	5	5	15
Coordinates (WGS 1984)	44.918403°N, 73.055664°W	44.444331°N, 73.214482°W	44.864468°N, 72.552904°W
Soil and surficial geology	Sandy, silty, and stony loams	Sand and silty loams, clay	Glacial till, sandy loam
Vegetation	Agricultural, mixed northern hardwoods and conifer	Urban/suburban landscaping, mixed northern hardwoods and conifer, agricultural	Mixed northern hardwoods and conifer

(C-Q) hysteresis patterns (Vaughan et al., 2017, 2019) in streams draining these different source areas. These C-Q patterns serve as a valuable proxy that provide novel insight into transport dynamics (e.g., Rose et al., 2018, and references therein). Together with accurate event-based nutrient yields, inferring transport dynamics from C-Q relationships can improve our understanding of controls on downstream N and P transport and the resulting stoichiometry in receiving waters.

In this study, we use a unique, 5-year high-frequency dataset consisting of more than 400 events to consider how LULC and seasonality alter event NO_3^- and SRP export dynamics from three low-order catchments with contrasting primary LULC (agricultural, forested, and urban). Previous work from these sites focused solely on dissolved organic carbon and NO_3^- export dynamics over event to annual time scales (Seybold et al., 2019; Vaughan et al., 2017, 2019). Building upon these previous studies that focused on carbon and N dynamics, our study leverages a novel approach to quantify stream SRP concentrations using in situ UV-visible spectrophotometer sensors (Vaughan et al., 2018) to concurrently monitor NO_3^- and SRP concentration dynamics. This allows direct comparison of the export dynamics and stoichiometric patterns for dissolved and immediately bioavailable nutrients over event and seasonal time scales. We start from the premise that event solute transport is the product of the interactions between event characteristics (water yield), LULC, and seasonal dynamics that will impact NO_3^- and SRP transport differently, influencing the timing, magnitude, and stoichiometry of event NO_3^- and SRP exports. We specifically hypothesize that (1) the timing and magnitude of event transport will differ between NO_3^- and SRP as a result of their different source areas and associated transport pathways, (2) LULC and seasonal dynamics will interact to further modify NO_3^- and SRP export patterns by influencing the spatial and temporal distributions of solute pools and connectivity in the landscape, and (3) the resulting differences in event NO_3^- and SRP export as a function of LULC and seasonal dynamics will drive divergent stoichiometric patterns among these sites and seasons.

2. Study Catchments

The study catchments were located in the Lake Champlain Basin of Vermont in the northeastern United States (Table 1 and Figure 1). Each catchment had a different primary LULC (agricultural, urban, or forested), were within a comparable range of catchment size, and were easily accessible for regular sensor maintenance and sampling. Hungerford Brook is a primarily agricultural (45%) catchment, including dairy production, row crops, hay, and pasture. Potash Brook is located near the city of Burlington, which is

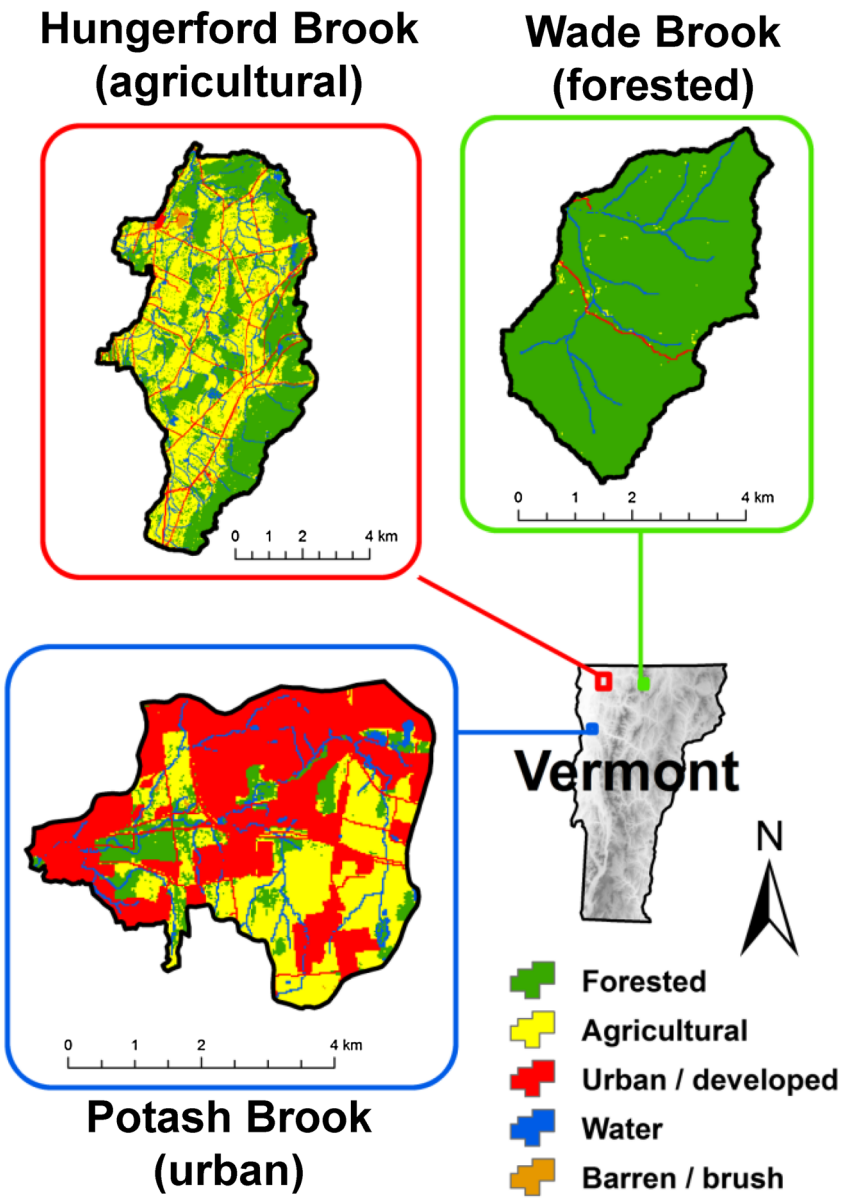

Figure 1. Map showing location and land use/land cover of the three study areas.

Vermont's densest population center. Its watershed is primarily characterized by urban and suburban development (54%) and includes some agricultural and forest cover (29% and 11%, respectively). The Wade Brook catchment is primarily forested (95%) and is situated on the western slope of Vermont's Green Mountain chain. Hungerford Brook and Wade Brook drain to the Missisquoi River and Lake Champlain; Potash Brook drains directly to Lake Champlain. Precipitation totals in the Wade Brook catchment (mean 1,453 mm yr^{-1}) are greater than the catchments of Hungerford Brook and Potash Brook (1,000 and 961 mm yr^{-1}, respectively) due to orographic effects (Table 1).

3. Methods

3.1. Lab Analysis of Grab Samples

Manual grab samples were collected at the sensor sites across the monitored seasons during baseflow and event flow and were timed to coincide with sensor measurements to calibrate in situ UV-visible absorbance spectra (see section 3.2) to laboratory NO_3^- and SRP concentration measurements. We analyzed 119–168

samples per site for NO_3^- and between 109–153 samples per site for SRP over the course of the study. The samples were collected across a range of event flow conditions (peak flow, rising, and falling limb) and discharge values. Maximum discharge values for events were within the range of discharge values captured by our sampling 92–99% of the time, depending on the site. Samples were filtered using 0.7-μm pore-size glass fiber (GF/F) filters (years 2014–2016) or 0.45-μm pore-size polyethersulfone membrane filters (years 2017–2018) into new HDPE bottles. Samples were frozen until lab analysis. We measured NO_3-N concentration using the open tubular cadmium reduction method following the QuickChem method 31-107-04-1E on a Lachat analyzer (years 2014–2016) or SEAL Analytical method G-172-96 on a SEAL AutoAnalyzer 3 (years 2017–2018). We measured SRP concentration colorimetrically (Shimadzu UV-2600 spectrophotometer) with the molybdate blue method consistent with US EPA method 365.1 (Parsons et al., 1984; years 2014–2016) or using the SEAL Analytical method G-297-03 on a SEAL AutoAnalyzer 3 (years 2017–2018).

3.2. In-Stream Measurements

We used s::can spectro::lyser UV-visible spectrophotometers (s::can Messtechnik GmbH, Vienna, Austria) to estimate NO_3^- and SRP concentrations in streams draining the catchments. The sensors were deployed in the stream from June 2014 to November 2018 from approximately mid-April through mid-November (Seybold et al., 2019). The spectrophotometers measured light absorbance at wavelengths from 220 to 750 nm at 2.5-nm intervals every 15 min. Optical path lengths were either 5 or 15 mm, depending on the typical turbidity of each stream (Table 1), and absorbance spectra were normalized by optical path length for comparison. The sensor measurement windows were automatically cleaned by a silicone wiper before each measurement and manually cleaned with pure ethanol at least every 2 weeks to prevent fouling and bioaccumulation. To focus on dissolved constituents, absorbance spectra were corrected for the effects of turbidity by fitting a third-order polynomial in the visible range of the spectrum, extrapolating into the UV portion, and then subtracting the extrapolated absorbance from the raw spectrum (Avagyan et al., 2014; Langergraber et al., 2003; Vaughan et al., 2017). Discharge data were acquired from a U.S. Geological Survey gaging station where available (Hungerford Brook Station 04293900), or calculated from stage-discharge rating curves developed with velocity-area calculations (Turnipseed & Sauer, 2010) and/or salt dilution (Moore, 2005). Stream stage was measured at 15-min time intervals at each site using atmospherically compensated pressure transducers.

3.3. Calibration of Absorbance Spectral Data to Estimate NO_3^- and SRP Concentrations

We estimated NO_3^- and SRP concentrations from calibration algorithms that related lab analyses of these solutes to the absorbance spectra of the same samples. We developed these algorithms using the partial least squares regression (PLSR) method detailed in Etheridge et al. (2014) and Vaughan et al. (2017) for NO_3^- and Vaughan et al. (2018) for SRP. The NO_3^-algorithm is based on relationships between measured NO_3^- concentrations and UV-visible absorbance of the NO_3^- molecule at a narrow range of specific wavelengths, allowing for use of a single NO_3^- calibration among sites (Etheridge et al., 2014; Vaughan et al., 2017). In contrast, the SRP algorithm is based on relationships between measured SRP concentrations and the UV-visible absorbance of a suite of constituents that varied consistently and in proportion with SRP concentrations. Because the constituents correlated with SRP could vary among sites/LULCs, individual calibration models were developed for each site (Vaughan et al., 2018). We used the pls package in R (Mevik et al., 2018; R Core Team, 2019) to generate calibration algorithms that were applied to the entire time series of absorbance spectra. PLSR models were calibrated for each site and analyte. Each model incorporated a number of components equal to the maximum of approximately 10% of the observations as recommended by Mevik et al. (2018). Model details and statistics are available as supporting information (Tables S1 and S2). Time series were generated by filling short data gaps (<2 hr) using linear interpolation. To estimate NO_3-N and SRP load (g s^{-1}), we multiplied predicted concentration by concurrent discharge (m^3 s^{-1}). The predicted SRP time series was inherently noisier than the NO_3^- time series at low baseflow concentrations preceding and following events, because these low concentrations were often at or near our detection limit. For this reason, when calculating hysteresis indices for events (see section 3.5), we smoothed the predicted SRP time series using a simple moving average with a rolling window of 2.25 hr to better capture average patterns of hysteresis loops (directionality and dimensions). See supporting information Figure S1 for an example of smoothed versus unsmoothed data.

3.4. Event Delineations

We delineated events using the HydRun package in MATLAB (Tang & Carey, 2017), which separates baseflow from event flow using the recursive digital filter technique proposed by Nathan and McMahon (1990). HydRun detects event start and end points based on user set flow thresholds. Flow thresholds were set individually for each catchment by manual tuning until HydRun event delineations were determined to be optimal (Table S3). We visually inspected hydrographs and HydRun event delineations alongside the predicted NO_3^- and rainfall time series and where necessary, manually modified event delineations in the following manner: (i) eliminated events not associated with a rainfall-runoff response and added events clearly missed by HydRun (both scenarios likely due to sensor noise or events were not detected by the fixed thresholds set in HydRun), (ii) revised the start point of an event if the selected point occurred before the rising limb of the hydrograph (likely due to sensor noise), (iii) revised the end point of an event if the selected point was visually too far beyond the inflection point of the falling limb of the hydrograph (a scenario possible given the HydRun algorithm dependence only on a recession threshold), and (iv) split an event into separate events if two hydrograph peaks could be clearly identified and associated with rainfall pulses separated by 12 or more hours.

3.5. Hysteresis Index Calculations and Analyses

We quantified event-based hysteretic behavior by calculating the hysteresis and flushing indices. Detailed methods describing the calculation of these indices, which were adapted from methods in Butturini et al. (2008) and Lloyd et al. (2016), can be found in Vaughan et al. (2017). We briefly describe these methods here.

Both indices are based on normalized discharge and parameter values (i.e., NO_3^- or SRP concentration):

$$Q_{i,norm} = \frac{Q_i - Q_{min}}{Q_{max} - Q_{min}} \tag{1}$$

$$C_{i,norm} = \frac{C_i - C_{min}}{C_{max} - C_{min}}, \tag{2}$$

where Q_i and C_i are the discharge and parameter values at time interval i, respectively; Q_{max} and C_{max} are maximum event values; and Q_{min} and C_{min} are minimum event values. This normalization method transforms discharge and parameter values from 0 to 1 and facilitates comparison of indices across events because all events are assessed on the same scale (Lloyd et al., 2016).

We calculated the hysteresis index at each discharge interval HI_j using the equation:

$$HI_j = C_{j,rising} - C_{j,falling}, \tag{3}$$

where $C_{j,rising}$ and $C_{j,falling}$ are found by estimating $C_{i,norm}$ at 1% intervals of $Q_{i,norm}$ on the rising and falling limbs through linear regression of two adjacent values $C_{i,norm}$. We calculated the mean of all HI_j values for the event to determine an overall hysteresis index for each event. Values of this index range from −1 to 1. Negative values indicate counterclockwise hysteresis, positive values indicate clockwise hysteresis, and the magnitude of HI indicates the normalized difference between the rising and falling limbs.

The event flushing index (FI) is equal to the normalized parameter value at the time of peak event discharge minus the normalized parameter value at the beginning of the event. Values of this index also range from −1 to 1. Negative values indicate a decrease in parameter value on the rising limb, positive values indicate an increase in parameter value on the rising limb, and the distance from zero indicates the magnitude of this difference.

3.6. NO_3^- and SRP Yield Calculations and Analyses

We integrated NO_3-N and SRP load for each event duration and the year to determine event and ice-free season (April–November) mass yields (kg N or P). To facilitate comparisons among sites, we calculated catchment-area normalized yield (kg N or P km^{-2}). We also integrated discharge for the year and each event to calculate the amount of runoff and then divided by catchment area to determine water yield (mm). To facilitate comparisons of solute yields among events with different water yields, we calculated

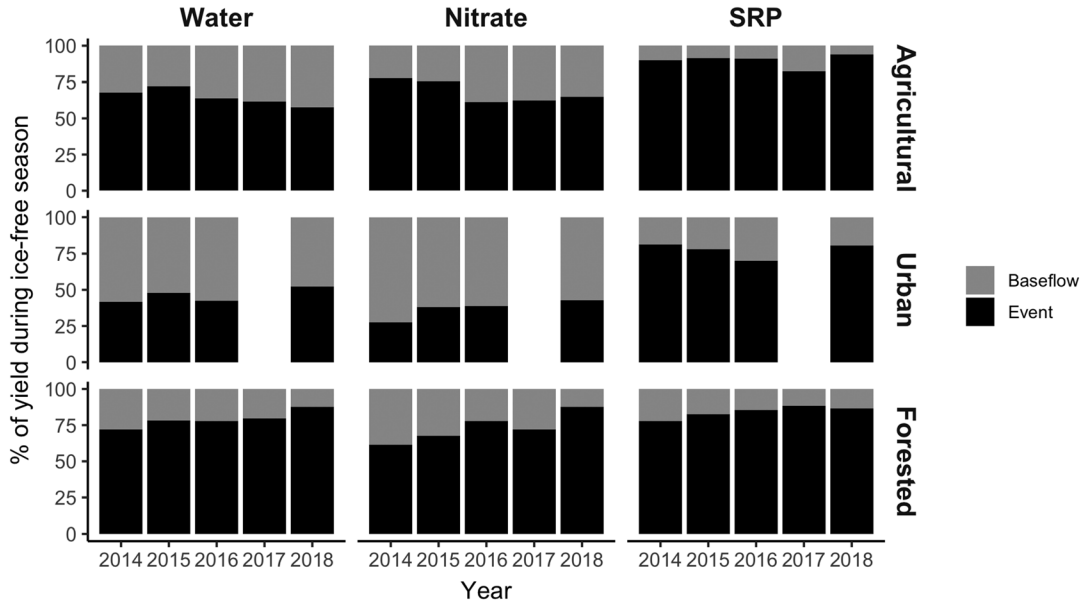

Figure 2. Percent contribution of baseflow and storm-event flow to ice-free season (April–November) yields of water (left), nitrate (middle), and soluble reactive P (SRP; right) for the agricultural (top), urban (middle), and forested (bottom) streams.

runoff-normalized yield (kg N or P L^{-1}) by dividing the total solute yield by total water yield for each event. It is conceptually analogous to a volume-weighted mean concentration (mass/flow volume), and it represents the average amount of NO_3-N and SRP mobilized per mm of runoff. To evaluate the relative composition of event NO_3^- and SRP exports and to facilitate stoichiometric comparisons, we calculated yield ratios by dividing event NO_3^- yield in moles by event SRP yield in moles. We were particularly interested in the Redfield N:P ratio of 16:1, a threshold generally used to indicate phytoplankton P-limitation (Smith, 2006).

To explore the relationships between event NO_3^- or SRP yield and water yield, we performed least squares linear regression for each site and solute grouping. When less than 90% of variance was explained, additional regressions were performed by grouping events by season. Because event NO_3^- and SRP yields are calculated using stream discharge, they are intrinsically autocorrelated with water yield. Thus, if solute concentration is constant, we expect a perfect linear correlation. A weak correlation indicates greater variability in solute concentration related to other factors besides stream discharge. Differences in correlation coefficients between sites or seasons arise from differences in solute concentrations during and among events. We compared correlation coefficients from these subgroups for statistical differences using a *z*-test (Paternoster et al., 1998). Models with correlation coefficients that were not significantly different were then tested for categorical differences using analysis of covariance (ANCOVA).

To test for differences in runoff-normalized yields and yield ratios (NO_3^- to SRP yield) among seasons at each site, we first conducted non-parametric Kruskal-Wallis rank sum tests for yields and ratios. Following the rejection of the null hypothesis ($\alpha = 0.05$), we conducted pairwise comparisons of yields and ratios with two-sided Conover-Iman tests ($\alpha = 0.05/2$). To control the false discovery rate we adjusted *p* values with the Benjamini-Hochberg procedure (Benjamini & Hochberg, 1995).

4. Results

4.1. Event Contributions to Annual NO_3^- and SRP Export

High flow events often contributed a greater annual proportion of water, NO_3^-, and SRP yields than did baseflow, though this was not the case for water and NO_3^- yields at the urban site (Figure 2). Event water yields at the agricultural and forested site ranged from 58% to 88% of ice-free season water yields across all years. Event water yields represented a smaller proportion of the ice-free season water yield at the urban

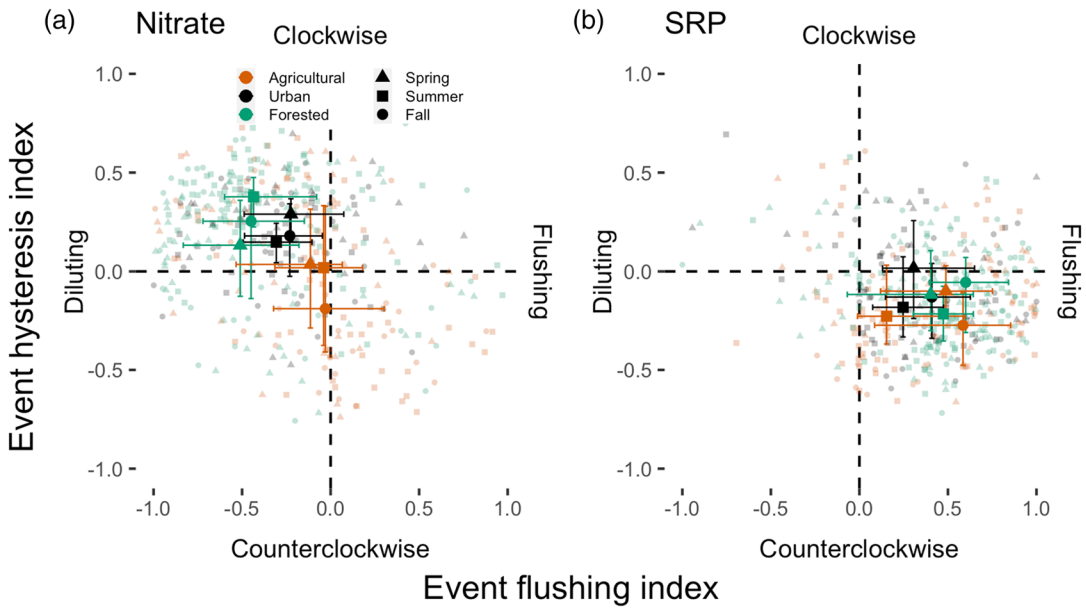

Figure 3. Event hysteresis and flushing index for nitrate (a) and soluble reactive P (b). Points are colored by site and shape represents season. The larger points represent the median for each group. Error bars represent the interquartile range.

site, contributing a maximum of 52% in 2018. Event contributions to NO_3^- loads were similar to those for water. Specifically, events contributed the majority of ice-free season NO_3^- yields at the agricultural and forested sites and less than 50% of ice-free season NO_3^- yields at the urban site. SRP yields were always disproportionately influenced by events regardless of land use. Event SRP yields ranged from 70% to 95% of ice-free season SRP yields.

4.2. Event Hysteresis Indices

The consistency of event NO_3^- hysteretic behavior differed among sites (Figure 3a). For both the urban and forested sites, 65% of events had positive HI and negative FI values for NO_3^-, indicating clockwise hysteresis with a diluting effect (decreasing concentrations on the rising limb). At the agricultural site, approximately one third of events had the same HI and FI combination for NO_3^- as the urban and forested sites (positive HI and negative FI), while another one third of events had the opposite behavior with negative HI (counterclockwise hysteresis) and a positive FI (flushing effect with increasing concentrations on the rising limb).

Hysteresis patterns were more consistent among sites for SRP and in general differed fundamentally from the patterns observed for nitrate (Figure 3b). The majority of events (84%) had positive FI values (flushing effect) for SRP. Of those events with a flushing effect, 75% had negative HI values (counterclockwise hysteresis). Site-specific examples of event time series (discharge and NO_3^- and SRP concentrations) for the dominant hysteretic behavior (NO_3^-: positive HI, negative FI; SRP: negative HI, positive FI) are available in supporting information (Figure S2).

4.3. Drivers of Event NO_3^- and SRP Exports

Despite variation in the hysteretic behavior of NO_3^- and SRP concentrations during individual events, event water yield generally explained a large proportion of the variance in event NO_3^- and SRP yield, but the magnitude of the response depended on the site and solute (Figures 4a and 4e). Event water yield explained >50% of the variance in solute yield for all site and solute groupings, except for SRP at the agricultural site ($R^2 = 0.40$; Figure 4e). The greatest solute yield per event water yield for both solutes occurred at the agricultural site. The magnitude of the slope of the linear relationships in Figures 4a and 4e at the agricultural site was 11 and 2 times greater (NO_3^- and SRP, respectively) than at the urban site and 15 and 22 times greater than at the forested site (see Table S4 for slope estimates).

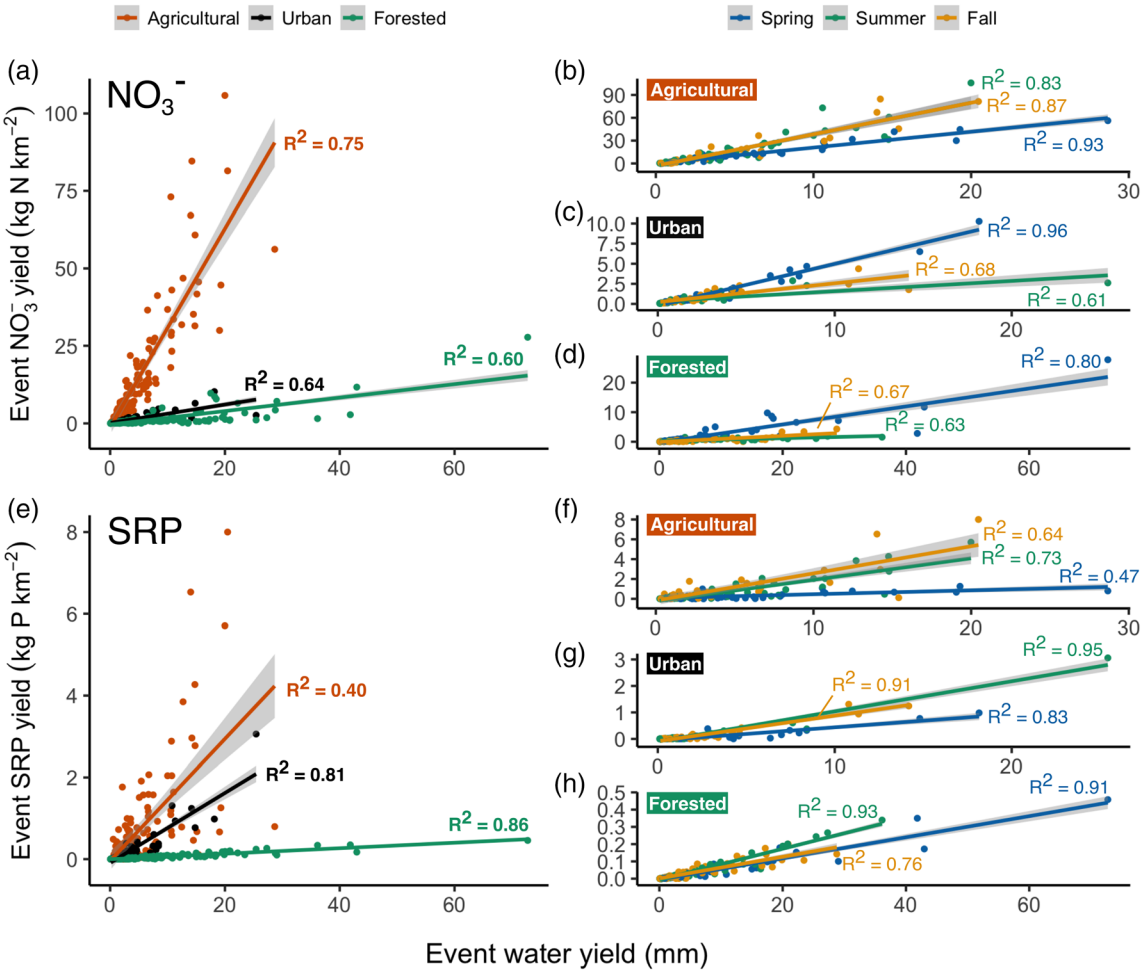

Figure 4. Event nitrate (NO_3^-; a–d) and soluble reactive P (SRP; e–h) yield versus event water yield for all 403 events observed during the 2014–2018 field seasons. Data are grouped by sites in the plots on the left. Data are separated by site and grouped by season in the plots on the right. Shaded regions indicate 95% confidence intervals. All relationships for data grouped by sites (a, e) were highly significant ($p < 0.0001$), and all slopes were significantly different when comparing responses for NO_3^- and SRP separately. All relationships for data grouped by season (a–d, f–h) were highly significant ($p < 0.0001$). All slopes for seasons were significantly different, except for summer and fall at the agricultural site for NO_3^- ($p = 0.97$) and SRP ($p = 0.15$) and spring and fall at the forested site for SRP ($p = 0.78$). ANCOVA tests also showed no significant differences for these regressions.

In general, a larger proportion of the variance in event NO_3^- and SRP yield was explained by event water yield when events were grouped by season (Figures 4b–4d and 4f–4h). Spring events exported the most NO_3^- per event water yield at the urban and forested sites but exported the least NO_3^- at the agricultural site (Figures 4b–4d and Table S4). Conversely, spring events exported the least amount of SRP per event water yield at all sites, though the spring and fall slopes at the forested site were not significantly different ($p = 0.78$; Figures 4f–4h and Table S4). Summer and fall relationships tended to be most similar for both NO_3^- and SRP, except for SRP at the forested site, though seasonal slopes were all similar at this site (0.006–0.009; Table S4).

Seasonal trends in runoff-normalized yields differed among sites and between solutes (Figures 5a and 5b). At the agricultural site, variability of runoff-normalized NO_3^- yields increased from spring to summer and fall, but not median yields. Conversely, median runoff-normalized SRP yields increased from spring to fall. At the urban site, median runoff-normalized NO_3^- yields decreased from spring to fall and SRP yields increased. At the forested site, runoff-normalized NO_3^- yields decreased from spring to fall but did not change for SRP.

4.4. Event NO_3^-:SRP Yield Ratios

Site and season influenced the relative contributions of NO_3^- and SRP to event yields (yield ratios; Figure 5c). When all seasons were grouped by site (not shown), the agricultural and forested sites had

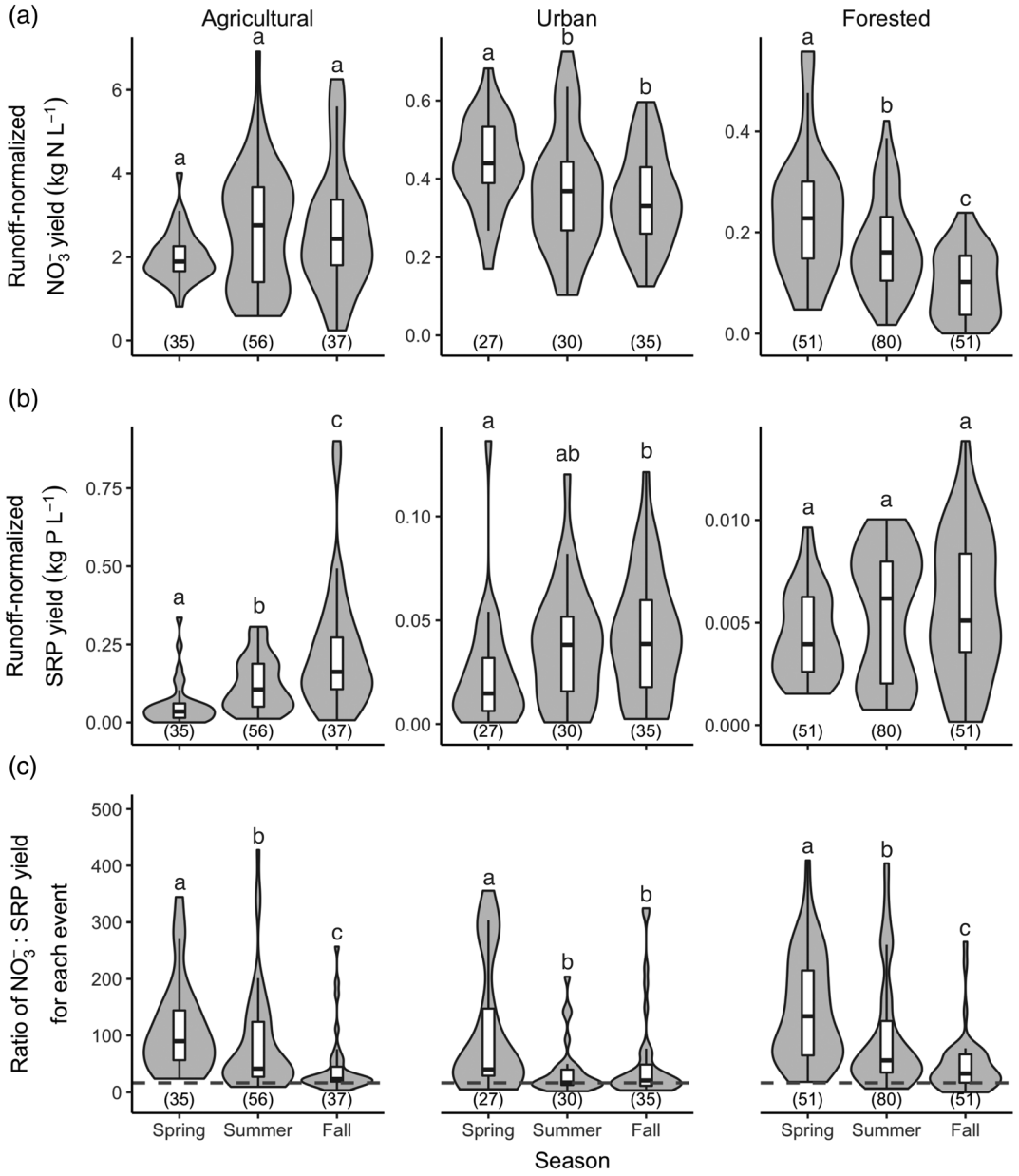

Figure 5. Plots (a) and (b) show runoff-normalized yields for nitrate (NO_3^-) and soluble reactive P (SRP), respectively. Note differences in vertical axis scales. Plot (c) shows the molar ratio of NO_3^- to SRP yield for each event. The dashed horizontal line in (c) shows the 16:1 molar N:P ratio. Not shown in (c), but included in the boxplot statistics, are 26 outlier points ranging from 542 to 27,105. Violin plots (shaded regions) represent the mirrored density distribution of the ratios. Boxplots within the violin plots represent the median and interquartile range. Numbers in parentheses are the number of observed events for each grouping. Letters above plots indicate statistical differences in medians according to post hoc comparisons of yields and ratios with two-sided Conover-Iman tests ($\alpha = 0.05/2$) within each land use/land cover.

greater median yield ratios (46 and 67, respectively) than the urban site (29; $p < 0.01$ and $p < 0.0001$, respectively). The greatest variability in yield ratios was observed at the forested site (interquartile range [IQR]= 138 NO_3^- to SRP) followed by the agricultural site (IQR = 108 NO3:SRP) and the urban site (IQR = 62 NO_3^- to SRP). When all sites were grouped by season (not shown), median yield ratios were greater in spring (100) than in summer (47; $p < 0.0001$) and greater in summer than in fall (27; $p < 0.0001$), though this trend depended on site (Figure 5c). Variability in yield ratios followed this same

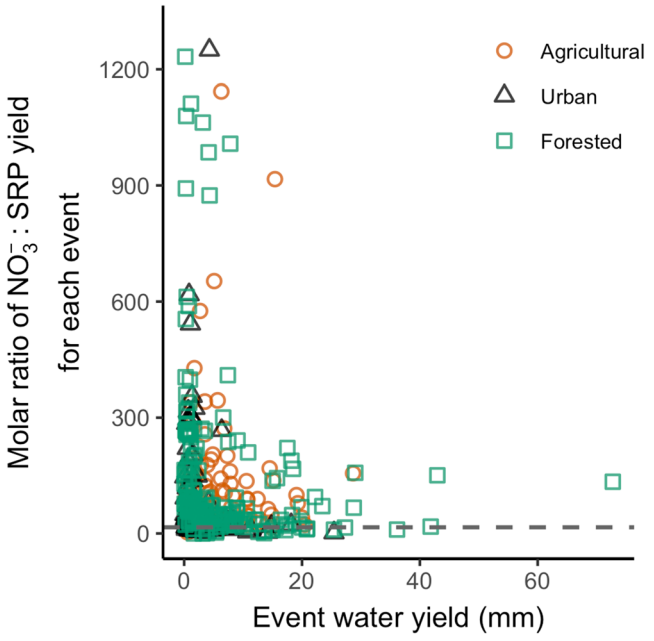

Figure 6. Molar ratio of nitrate (NO_3^-) to soluble reactive P (SRP) yield for each event. The dashed horizontal line shows the 16:1 molar N:P ratio. Not shown are eight outliers with ratios from 1,517 to 27,105 between 0.11 and 3.03 mm event water yield. An alternate figure depicting data colored by season instead of site is available in supporting information (Figure S3).

seasonal trend with the greatest variability in spring (IQR = 170 NO_3^- to SRP) and the least in the fall (IQR = 52 NO_3^- to SRP). In general, median yield ratios became closer to the Redfield N:P ratio of 16 as the seasons progressed (Figure 5c). Conversely, the median molar NO_3^-:SRP ratio during baseflow conditions was >130 at all sites, above the 16:1 ratio. There was no obvious relationship between NO_3^-:SRP yield ratios and event water yield at any site (Figure 6). However, smaller events (<10 mm event water yield) had the greatest variability and highest yield ratios at all sites.

5. Discussion

While high-frequency sensor data have been used to examine export patterns and drivers of solutes including NO_3^- (Koenig et al., 2017; Seybold et al., 2019; Vaughan et al., 2017), this study is one of the first to use a multi-year high-frequency SRP time series to concurrently examine event-scale export dynamics of two key determinants of water quality (see also Frazar et al., 2019). Further, and perhaps most notably, our analysis of sensor-derived time series combines classic concentration-discharge and hysteretic frameworks with stoichiometry to link hydrobiogeochemical and ecological processes. This approach provided novel insights into how LULC and seasonality drive nutrient export from catchments and how these drivers interact to produce seasonal patterns in stream chemistry that may influence ecological processes, such as productivity, in receiving waters.

5.1. Different Mechanisms for NO_3^- and SRP Mobilization

Our multi-year high-frequency time series of NO_3^- and SRP concentrations captured >400 high-flow events and provides unique insight into event NO_3^- and SRP transport dynamics and how these were impacted by site and solute-specific source areas and/or transport pathways. We found that NO_3^- and SRP were mobilized differently during events. Specifically, SRP mobilization is more frequently transport limited than NO_3^-. We infer transport limitation of SRP in two ways. First, the majority of SRP yield during the ice-free season occurs during event flow rather than baseflow at all sites regardless of the contribution of event flow to total annual water yields (Figure 2). Second, and supporting the first, is that the majority of events at all sites had counterclockwise HIs and positive FIs for SRP (Figure 3), where SRP concentrations were greater at peak flow than at event flow onset. This export behavior has been reported as the dominant behavior for SRP in several catchments (Bowes et al., 2005; Dupas et al., 2015; Frazar et al., 2019; Rose et al., 2018), though not all (Bieroza & Heathwaite, 2015; Bowes et al., 2015; Outram et al., 2014; Siwek et al., 2012). Our conclusion is further supported by studies that demonstrate that most dissolved P is exported after discharge surpasses a critical threshold (Rose et al., 2018; Underwood et al., 2017). Above this threshold, hydrologic connectivity is established between the stream and subsurface flowpaths, and SRP is laterally transported from upper soil depths where P is typically more concentrated than at deeper depths (Siwek et al., 2012).

In contrast, the hysteresis patterns of NO_3^- suggest the dominant transport pathways differ from those for SRP. Unlike SRP, the majority of events among all land uses had clockwise HI and negative FI for NO_3^- (Figure 3). These indices imply the initial NO_3^- source, likely shallow groundwater within the stream or riparian network, is progressively depleted and/or diluted by less concentrated source waters, such as overland flow and/or water from riparian wetlands with low NO_3^- concentrations, as the event saturates the catchment and generates runoff from more distant sources. These results suggest event NO_3^- and SRP transport dynamics are frequently decoupled at our sites, with highest SRP concentrations mainly exported towards the end of the events with mobilized soil water and highest NO_3^- concentrations generally exported towards the beginning of events with shallow groundwater. The greater importance of groundwater for NO_3^- compared to SRP transport has been reported in other catchments (Frazar et al., 2019; Vanni et al., 2001) and is further supported at our study sites by the correspondence between baseflow

contributions (primarily groundwater) to annual yields of water and NO_3^- (Figure 2). The proportion of NO_3^- transported by baseflow closely mirrors that of water at each site, whereas the vast majority of SRP transport occurred during event flow at all sites. Similar decoupled transport has been observed in an agricultural and an urban catchment in Rhode Island, USA (Frazar et al., 2019). Conversely, and unlike at our forested site, studies in relatively undeveloped headwater streams in Ontario, Canada, and the northeastern United States found that NO_3^--discharge relationships were positive and transport-limited NO_3^- flushing was common in forested catchments (Creed et al., 1996; Inamdar et al., 2004; Koenig et al., 2017). Thus, drivers of NO_3^- transport behavior in less developed catchments may be more complicated than in human-dominated LULCs and may include other catchment properties (e.g., atmospheric deposition chemistry, precipitation/snowmelt variability, elevation, local soil and bedrock properties, vegetation, proportion of wetland cover, etc.).

5.2. LULC Modifies NO_3^- and SRP Exports

At our study sites, LULC drove differences in NO_3^-, but not SRP hysteresis patterns (Figure 3). This was especially evident for NO_3^- hysteresis patterns at the agricultural site. While the majority of events had clockwise HI and negative FI values for NO_3^-, at the agricultural site approximately one third of events from each season had the opposite hysteretic behavior (counterclockwise HI and positive FI). Variability of NO_3^- hysteresis patterns has been reported in other agricultural catchments (Bowes et al., 2015; Darwiche-Criado et al., 2015; Fovet et al., 2018; Outram et al., 2014; Rose et al., 2018), most likely because land use practices such as fertilization, artificial drainage, and irrigation alter the dominant sources and flowpaths for NO_3^- export among different agricultural catchments and within a given agricultural catchment over time (Bowes et al., 2015; Darwiche-Criado et al., 2015; van Herpe & Troch, 2000). For example, counterclockwise hysteresis and flushing export behavior might occur shortly after fertilizer applications, when topsoil NO_3^- concentrations surpass those of shallow groundwater concentrations. Thus, conditions can align in agricultural catchments to shift NO_3^- transport from supply limitation typical of forested catchments to transport limitation, as is the predominant case in other agricultural catchments (Oeurng et al., 2010; Outram et al., 2016; van Herpe & Troch, 2000).

LULC also drove differences in event NO_3^- and SRP yield relationships with event water yield (Figure 4 and Table S4). As expected, agricultural event yields were 15 and 22 times greater than forested for NO_3^- and SRP, respectively (Figures 4a–4b and 5a–5b and Table S4). This finding is consistent with literature demonstrating that agricultural practices enrich soil NO_3^- and SRP pools, increasing NO_3^- and SRP yields relative to less disturbed forests (Dubrovsky et al., 2011; Poor & McDonnell, 2007; Seybold et al., 2019; Vaughan et al., 2017). Urban event yields were 1.4 and 12 times greater than forested for NO_3^- and SRP, respectively (Figures 4a and 5a and Table S4). Unexpectedly, site differences were much smaller for event NO_3^- yields than SRP yields (Figures 4b and 5b) even though N loading to urban landscapes is typically greater than P loading (Hobbie et al., 2017). Lower than expected event NO_3^- yields from our urban catchment may result from permanent removal of NO_3^- via denitrification in stormwater control structures (Bettez & Groffman, 2012) and urban wetlands (Harrison et al., 2011). Further, because groundwater is an important NO_3^- transport pathway, the reduced importance of event flow to urban NO_3^- yields may result from the greater importance of baseflow to water yields at this site (Figure 2). The dominance of baseflow to water and NO_3^- yields has been observed in other urban catchments (Frazar et al., 2019; Janke et al., 2013) and can be attributed to either groundwater infiltrating drainage pipes located below the water table and/or surface water inputs from upstream wetlands. Wetlands comprise 12.4% of our urban catchment area (Table 1); thus, both groundwater and surface water connections could be contributing to baseflow at the urban site. However, because wetlands are typically NO_3^- sinks at lower flows (Cheng & Basu, 2017; Jordan et al., 2011) and should therefore be a dilute NO_3^- source, it is likely that most NO_3^- is transported to the urban stream via groundwater rather than surface water pathways. That said, it is important to note that the city in which our urban site is situated, while one of the largest municipalities in Vermont, has a relatively low population density (~450 people per km^2 or about 15% of the population density of Baltimore, Maryland, USA, the nearest urban site of the National Science Foundation's Long-term Ecological Research Network). As such our urban site may be more representative of catchments in developed areas with lower population densities (i.e., suburban) and less representative of catchments in major urban centers.

Unlike NO_3^-, event flow contributed disproportionately to urban SRP yields (Figure 2). This difference results from the distinct transport pathways for NO_3^- and SRP. Because it readily adsorbs to porous media, SRP is much less mobile than NO_3^-, and subsurface pathways, such as those that contribute to baseflow, are typically enriched with N relative to P (Hobara et al., 2005; Holtan et al., 1988). Conversely, the majority of dissolved P is mobilized after discharge surpasses a critical threshold during events (Rose et al., 2018; Underwood et al., 2017). Furthermore, elevated event SRP yields at the urban site relative to the forested site (Figures 4e and 5b) are likely due to increased human inputs and modified transport pathways (e.g., impervious surfaces and event drains) that limit the capacity for biology to retain and soils to immobilize P (Hobbie et al., 2017, and references therein). Thus, LULC, specifically agriculture and urbanization, modify NO_3^- and SRP export dynamics by impacting both nutrient availability and how water and nutrients move through and interact with landscapes.

5.3. Season Modifies NO_3^- and SRP Exports

Seasonal dynamics also exert a strong and distinct control on event NO_3^- and SRP yields at each site. At the urban and forested sites, event NO_3^- yields were generally greater in spring than in summer or fall (Figures 4c–4d and 5a). Elevated event NO_3^- yields in spring at the forested site highlight temporal imbalances between NO_3^- production, biological demand, and transport. Insulated soils underlying snowpack, which is maintained much of the winter at the forested site, promote nitrification of soil N that accumulates in the catchment when biological demand is low and transport is typically limited (Brooks et al., 1998; Campbell et al., 2006). Prior to increased biological demand in late spring, snowmelt and seasonal rains transport this accumulated NO_3^- to the stream (Campbell et al., 2006; Pellerin et al., 2012; Piatek et al., 2005; Sebestyen et al., 2008). While similar dynamics may contribute to elevated NO_3^- yields in spring at the urban site, snowpack is not as persistent at this site and soils are more prone to freezing, another process that can promote N losses from soils. Soil freezing and thawing cycles can kill fine roots, lyse microbial cells, and physically disrupt soil aggregates and fragment fresh plant litter, processes that can increase soil solution N and/or reduce biotic N assimilation by fine roots and promote leaching losses of NO_3^- from soils in spring runoff (Campbell et al., 2014; Fitzhugh et al., 2001; Mitchell et al., 1996; Watmough et al., 2004), though not always (Fitzhugh et al., 2003; Fuss et al., 2016; Judd et al., 2010). Additionally, anthropogenic inputs such as accumulated pet waste (Hobbie et al., 2017) could contribute to increased NO_3^- concentrations in spring runoff at the urban site. Regardless of the source of accumulated N in late winter/early spring, biological demand for N is low and NO_3^- is available for transport when hydrologic flux is greatest (Seybold et al., 2019).

Conversely, at both forested and urban sites, elevated biological demand during the warm summer and early fall seasons reduce NO_3^- available for event transport. Warmer temperatures and reduced hydrological connectivity increase biogeochemical reaction rates and residence times (Hrachowitz et al., 2016), favoring plant NO_3^- uptake and denitrification, thereby reducing NO_3^- concentrations in event runoff. In contrast to seasonal patterns at the urban and forested sites, event NO_3^- yields at the agricultural site were generally greater in summer and fall than in spring (Figures 4b and 5a). As Vaughan et al. (2017) observed at this site, these patterns likely arise from agricultural land use practices, specifically manure and fertilizer applications that begin in mid- to late-spring and are often repeated in fall, resulting in elevated runoff-normalized NO_3^- yields in early summer and late fall.

Similar seasonal SRP export patterns were observed at all of the sites (Figures 4f–4h and 5b), with greater yields occurring in summer and fall than in spring, though the difference was minimal at the forested site and most apparent at the agricultural site. The lack of a strong seasonal SRP yield pattern at the forested site is likely due to a lack of available P (Figures 4e and 5b), as P limitation of trees has recently been reported in hardwood forests of the northeastern United States (Goswami et al., 2018). Seasonal patterns at the agricultural site reflect those we observed for NO_3^- and likely arise from agricultural manure and fertilizer applications that increase event SRP yields in summer and fall. Fall events at the agricultural site had even greater runoff-normalized SRP yields than summer, perhaps driven by reduced crop uptake after fall harvest and late season P-enriched manure applications (Downing & McCauley, 1992; Reckhow et al., 1980) that are common prior to the required winter ban on manure application. Further, the weakest seasonal correlations between event SRP yield and water yield occurred at the agricultural site (Figure 4f), indicating that event SRP concentrations are more variable and less predictable than in other LULCs. The increased variability may result from temporal and spatial variability in fertilizer applications, as well as other agricultural

practices that alter the hydrology of catchments by impacting evapotranspiration and drainage rates (e.g., by installing tile drainage systems).

Even though seasonal differences in SRP yields were smaller in the urban and forested catchments (Figures 4g–4h and 5b), the greatest event SRP yields tended to occur in summer and fall. During these seasons, higher temperatures and evapotranspiration promote dry soil conditions between events. Several studies have observed that wetting events generate greater soil porewater SRP concentrations and SRP yield following dry periods than following wet (Bowes et al., 2005; Gu et al., 2017; Stutter et al., 2008; Turner & Haygarth, 2001). As such, periodic dry periods may facilitate greater event SRP export during summer and fall. Conversely, more rapid surface and subsurface flows during the wet spring period result in reduced SRP concentrations in runoff when transport rates likely surpass the rate of PO_4^{3-} release from soils. Increased summer and fall SRP yields may also be sourced from water-saturated riparian wetland soils. Warmer temperatures and water-saturated soils drive reduced redox conditions in riparian wetlands, promoting the reductive dissolution and mobilization of SRP from wetlands (Dupas et al., 2018; Gu et al., 2017; Hoffmann et al., 2009; Surridge et al., 2007). Thus, the same seasonal physicochemical conditions in riparian wetlands that promote NO_3^- removal promote SRP mobilization.

5.4. Event NO_3^-:SRP Yield Ratios

Consistent with our hypotheses, LULC and seasonality interacted to alter the magnitude and timing of event NO_3^- and SRP exports (Figures 5a and 5b). However, despite considerable differences in catchment characteristics that led to different export dynamics, our results unexpectedly demonstrate that these interactions generated event NO_3^-:SRP yield ratios with similar seasonal patterns among sites (Figure 5c). One potential driver of seasonal declines in the variability and magnitude of yield ratios might be seasonal shifts in soil moisture and thus hydrologic connectivity in the catchments from spring to fall. In the spring, catchment soils are wettest and upland connectivity to the stream channel is greatest in terms of areal extent and temporal frequency (Jencso et al., 2009; Stieglitz et al., 2003). Consequently, multiple sources and flowpaths are engaged, and variability in terrestrial biogeochemistry is reflected in more variable stream water chemistry and corresponding N:P ratios (Frost et al., 2009; Green & Finlay, 2010; Green & Wang, 2008). As the catchments transition to drier periods in summer and fall, stream connectivity to uplands becomes more temporally sporadic and spatially heterogeneous, and stream water chemistry is reflective of fewer near-stream sources and flowpaths (e.g., riparian wetlands, shallow groundwater, and stream channels); consequently, stream water N:P ratios are less variable.

The seasonal decline in the magnitude of NO_3^-:SRP yield ratios we observed at our sites is also the consequence of seasonal shifts in hydrologic connectivity. Green and Finlay (2010) found that stream water N:P ratios tended to decline from late winter/early spring to fall in minimally impacted catchments as a result of decreasing hydrologic connectivity and increasing nutrient demand dynamics. Similarly, they posited that elevated N (relative to P) in stream water in earlier months results from persistent transport via soil water, a pathway more conducive to N transport because of the sorptive nature of P (Green et al., 2007). This supports the pattern we observed at our less impacted forested site. However, we would also add that NO_3^- depletion in fall storms at the forested site might also be due to the pulse of tree litter inputs at this time that provide a fresh source of carbon that requires external N to decompose (Goodale et al., 2009; Sebestyen et al., 2014; Sobczak et al., 2003; Webster et al., 2009).

Surprisingly, despite generally higher event NO_3^- and SRP yields at the more human-impacted urban and agricultural sites, event NO_3^-:SRP yield ratios at these sites spanned similar ranges as the forested site and also declined seasonally. One notable difference is the less prominent seasonal decline and slightly reduced variability in yield ratios at the urban site as compared to the forested and agricultural sites. Unlike in more intact forested systems, natural temporal variability in solute sources and flowpaths in urban systems can be overridden by the engineered dynamics of these managed landscapes (Groffman et al., 2014; Kaye et al., 2006). We posit that the muted seasonal signal and reduced variability at the urban site is likely due to homogenization of N and P export with landscape homogenization. As such, more densely populated and engineered urban systems than our site might have even less variability and lack a seasonal signal.

It is perhaps most surprising that we observed the seasonal decline in yield ratios at the agricultural site because these landscapes are so heavily managed. The seasonal event NO_3^- and SRP yield patterns at the

agricultural site are different than the other two sites (Figure 5), and we suggest this indicates that the seasonal decline in NO_3^-:SRP yield ratios is reflective of a unique combination of seasonally shifting drivers. The N-enriched yield ratios in spring may result from similar dynamics that drive yield ratios at the forested and urban site, namely, increased hydrologic connectivity with source areas and dominance of soil water transport. However, the seasonal decline in summer and spring, driven by P-enriched yields, likely results from a heavily concentrated source input, specifically manure. Manure, the most common agricultural input in Vermont, typically has a N:P ratio lower than the Redfield ratio of 16:1 (Downing & McCauley, 1992; Reckhow et al., 1980). Thus, P-enriched yields in summer and fall are reflective of mid- to late-spring and fall manure applications to fields. However, these patterns may be modified by different climate regimes and different inputs (e.g., more inorganic fertilizer with a higher N:P ratio) and thus generate different seasonal patterns of yield ratios.

Our results suggest that hydrologic connectivity is an important driver of event NO_3^-:SRP yield ratios at the seasonal scale and an important driver at the event scale. At the event scale, hydrologic connectivity to distinct NO_3^- and SRP sources is a function of rainfall or event magnitude and corresponding flow state or discharge, and thus, events of different magnitudes drive event NO_3^-:SRP yield ratios. At all sites, larger events had less variability and lower yield ratios than smaller events (Figure 6), a phenomenon that has been observed in other catchments (Correll et al., 1999; Green & Finlay, 2010; Green et al., 2007). Smaller events, especially when antecedent soil moisture is low, establish little or no connectivity and as such only activate near-stream sources, mobilizing more NO_3^- (e.g., from shallow groundwater) than SRP. As discharge increases, connectivity between the stream and subsurface flowpaths that transport SRP from upper soil depths is also established (Rose et al., 2018; Siwek et al., 2012; Underwood et al., 2017) and yield ratios decline. Additionally, higher event discharges mobilize P-rich particulates capable of releasing additional dissolved P (Correll et al., 1999; Underwood et al., 2017), further driving down NO_3^-:SRP yield ratios. The remarkable variation of NO_3^-:SRP yield ratios during small events is likely due to antecedent conditions (e.g., soil moisture), which influence the spatial and temporal availability of water and nutrients and the hydrologic flowpaths activated (e.g., McMillan et al., 2018, and references therein). Consequently, this source area variability is reflected in the magnitude and nutrient composition of runoff. Expanded monitoring networks capable of capturing the activation of variable source areas across soil-stream continua in response to combinations of different events and antecedent conditions would be the logical next step to exploring these dynamics.

While each of our catchments is a representative member of a given LULC classification in Vermont, they do not represent the full range of these LULCs and are not paired catchments that isolate LULC effects. Variable catchment properties, such as scale, atmospheric deposition chemistry, precipitation/snowmelt variability, elevation, local soil and bedrock properties, vegetation, proportion of impervious or wetland cover, and population density, can all impact hydrologic and biogeochemical responses and certainly shape our results. Furthermore, across managed landscapes, heterogeneity in how (i.e., agricultural best management practices or nutrient amendment policy, stormwater control) and where (i.e., development in riparian vs. upland watershed regions) the landscape is modified by human activities will also heavily impact from where and under what conditions these solutes are exported, which will likely further promote variability within LULC classes (e.g., Seybold et al., 2019). Regardless of LULC, our results suggest that smaller flow events will interact with antecedent conditions to produce the greatest variability in event stoichiometry. While our particular findings are not likely representative of how these LULCs will necessarily impact event stoichiometry in every case, they constitute a poignant and novel example of how LULC and seasonality can interact and impact the timing, magnitude, and relative export of NO_3^- and SRP. Importantly, this study illustrates insight gleaned from this new capacity to explore their coupled versus decoupled export across a range of catchment conditions, and the catchment research community can and should leverage this approach in the future to explore these dynamics across a diverse range of catchment conditions.

5.5. Implications for Receiving Waters and Management

In receiving waters, such as lakes, catchment loading and ratios of N and P influence ecological processes, including the likelihood of cyanobacterial blooms (Smith, 1983). In the Lake Champlain Basin, research has demonstrated that catchment N and P loading is an important driver of lake N and P dynamics, and declines in the TN:TP ratio are associated with increases in cyanobacteria (Isles

et al., 2017). Thus, the integrity of receiving ecosystems, including Lake Champlain, may be impacted by shifts in the timing and N to P stoichiometry of catchment exports, particularly during high flow events. Climate change in the northeastern United States will likely shift the timing of snowmelt and spring precipitation, resulting in increased NO_3^- yields earlier in the year. Subsequent exports will likely have lower N:P ratios (Figure 5c), potentially driving lake N:P ratios down and creating more favorable conditions for cyanobacteria earlier in the growing season than historically observed (Isles et al., 2017). Additionally, the persistence and intensity of precipitation events are projected to increase in the northeastern United States (Guilbert et al., 2015). These changes in precipitation may increase both the magnitude of event N and P yields (Figure 4) and lower event N:P yield ratios (Figure 6; Frazar et al., 2019; Gao et al., 2014). Both of these scenarios could impact lake productivity and possibly favor cyanobacteria blooms.

To reduce dissolved N and P transport to downstream ecosystems, our results suggest managers should prioritize reduction strategies specific to the nutrient, LULC, and season. For example, SRP in the urban catchment was primarily exported to the stream via event flow. As such, dissolved P reduction strategies should increase stormwater infiltration to promote P immobilization by soils. However, we caution that stormwater ponds, a popular nutrient management strategy, should be designed and maintained to avoid subsequent release of dissolved P (Taguchi et al., 2020). Conversely, because NO_3^- was mostly exported via baseflow at the urban site, strategies to reduce dissolved N export should restore riparian areas and build engineered structures that promote denitrification of stormwater (e.g., wet ponds and dry detention ponds) prior to infiltration. In the agricultural catchment, N and P transport patterns more frequently aligned, suggesting the dominant source and transport pathways were more similar (e.g., from fertilizer and manure). In this case, reduction strategies will likely impact both nutrients and may include restoring wetlands and floodplains to promote N and P removal. Additional strategies in agricultural catchments should target seasonal hot moments of export when uptake by crops is limited. These might include planting winter cover crops and limiting fall manure application.

Acknowledgments

This research was made possible through support from the National Science Foundation under VT EPSCoR grants OIA 1556770 and EPS-IIA 1330446. James Shanley and Andrew Vermilyea contributed to the conceptual development of this research. Saul Blocher and Ryan Sleeper assisted with installing and maintaining the sensor network and lab analyses. Scott Hamshaw assisted with event delineations. We appreciate thoughtful reviews from three anonymous reviewers that greatly improved this work. The data used in this publication are freely available on HydroShare (https://doi.org/10.4211/hs.85fa32a11fbb49779033934a135f54ef) and cited in the references (Kincaid et al., 2020).

References

Avagyan, A., Runkle, B. R. K., & Kutzbach, L. (2014). Application of high-resolution spectral absorbance measurements to determine dissolved organic carbon concentration in remote areas. *Journal of Hydrology*, *517*(C), 435–446. https://doi.org/10.1016/j.jhydrol.2014.05.060

Benjamini, Y., & Hochberg, Y. (1995). Controlling the false discovery rate: A practical and powerful approach to multiple testing. *Journal of the Royal Statistical Society. Series B*, *57*(1), 289–300.

Bernhardt, E. S., Band, L. E., Walsh, C. J., & Berke, P. E. (2008). Understanding, managing, and minimizing urban impacts on surface water nitrogen loading. *Annals of the New York Academy of Sciences*, *1134*(1), 61–96. https://doi.org/10.1196/annals.1439.014

Bettez, N. D., & Groffman, P. M. (2012). Denitrification potential in stormwater control structures and natural riparian zones in an urban landscape. *Environmental Science & Technology*, *46*(20), 10,909–10,917. https://doi.org/10.1021/es301409z

Bieroza, M. Z., & Heathwaite, A. L. (2015). Seasonal variation in phosphorus concentration-discharge hysteresis inferred from high-frequency in situ monitoring. *Journal of Hydrology*, *524*(C), 333–347. https://doi.org/10.1016/j.jhydrol.2015.02.036

Bowes, M. J., House, W. A., Hodgkinson, R. A., & Leach, D. V. (2005). Phosphorus–discharge hysteresis during storm events along a river catchment: The River Swale, UK. *Water Research*, *39*(5), 751–762. https://doi.org/10.1016/j.watres.2004.11.027

Bowes, M. J., Jarvie, H. P., Halliday, S. J., Skeffington, R. A., Wade, A. J., Loewenthal, M., et al. (2015). Characterising phosphorus and nitrate inputs to a rural river using high-frequency concentration–flow relationships. *Science of the Total Environment*, *511*(C), 608–620. https://doi.org/10.1016/j.scitotenv.2014.12.086

Brooks, P. D., Williams, M. W., & Schmidt, S. K. (1998). Inorganic nitrogen and microbial biomass dynamics before and during spring snowmelt. *Biogeochemistry*, *43*(1), 1–15. https://doi.org/10.1023/a:1005947511910

Butturini, A., Alvarez, M., Bernal, S., Vázquez, E., & Sabater, F. (2008). Diversity and temporal sequences of forms of DOC and NO_3-discharge responses in an intermittent stream: Predictable or random succession? *Journal of Geophysical Research*, *113*, G03016. https://doi.org/10.1029/2008JG000721

Campbell, J. L., Mitchell, M. J., & Mayer, B. (2006). Isotopic assessment of NO_3^- and SO_4^{2-} mobility during winter in two adjacent watersheds in the Adirondack Mountains, New York. *Journal of Geophysical Research*, *111*, G04007. https://doi.org/10.1029/2006JG000208

Campbell, J. L., Socci, A. M., & Templer, P. H. (2014). Increased nitrogen leaching following soil freezing is due to decreased root uptake in a northern hardwood forest. *Global Change Biology*, *20*(8), 2663–2673. https://doi.org/10.1111/gcb.12532

Cheng, F. Y., & Basu, N. B. (2017). Biogeochemical hotspots: Role of small water bodies in landscape nutrient processing. *Water Resources Research*, *53*, 5038–5056. https://doi.org/10.1002/2016WR020102

Core Team, R. (2019). *R: A language and environment for statistical computing*. Vienna, Austria: R Foundation for Statistical Computing.

Correll, D. L., Jordan, T. E., & Weller, D. E. (1999). Transport of nitrogen and phosphorus from Rhode River watersheds during storm events. *Water Resources Research*, *35*(8), 2513–2521. https://doi.org/10.1029/1999WR900058

Creed, I. F., Band, L. E., Foster, N. W., Morrison, I. K., Nicolson, J. A., Semkin, R. S., & Jeffries, D. S. (1996). Regulation of nitrate-N release from temperate forests: A test of the N flushing hypothesis. *Water Resources Research*, *32*(11), 3337–3354. https://doi.org/10.1029/96WR02399

Darwiche-Criado, N., Comín, F. A., Sorando, R., & Sánchez-Pérez, J.-M. (2015). Seasonal variability of NO_3^- mobilization during flood events in a Mediterranean catchment: The influence of intensive agricultural irrigation. *Agriculture, Ecosystems and Environment*, *200*, 208–218. https://doi.org/10.1016/j.agee.2014.11.002

Davidson, K., Gowen, R. J., Tett, P., Bresnan, E., Harrison, P. J., McKinney, A., et al. (2012). Harmful algal blooms: How strong is the evidence that nutrient ratios and forms influence their occurrence? *Estuarine, Coastal and Shelf Science*, *115*(C), 399–413. https://doi.org/10.1016/j.ecss.2012.09.019

Dhillon, G. S., & Inamdar, S. (2013). Extreme storms and changes in particulate and dissolved organic carbon in runoff: Entering uncharted waters? *Geophysical Research Letters*, *40*, 1322–1327. https://doi.org/10.1002/grl.50306

Downing, J. A., & McCauley, E. (1992). The nitrogen: Phosphorus relationship in lakes. *Limnology and Oceanography*, *37*(5), 936–945. https://doi.org/10.4319/lo.1992.37.5.0936

Driscoll, C. T., Whitall, D., Aber, J., Boyer, E., Castro, M., Cronan, C., et al. (2003). Nitrogen pollution in the northeastern United States: Sources, effects, and management options. *Bioscience*, *53*(4), 357–374. https://doi.org/10.1641/0006-3568(2003)053[0357:NPITNU]2.0.CO;2

Duan, S., Kaushal, S. S., Groffman, P. M., Band, L. E., & Belt, K. T. (2012). Phosphorus export across an urban to rural gradient in the Chesapeake Bay watershed. *Journal of Geophysical Research*, *117*, G01025. https://doi.org/10.1029/2011JG001782

Dubrovsky, N. M., Burow, K. R., Clark, G. M., Gronberg, J. M., Hamilton, P. A., Hitt, K. J., et al. (2011). The quality of our nation's waters: Nutrients in the nation's streams and groundwater, 1992–2004. *U.S. Geological Survey Circular*, *1350*, 1–174.

Dupas, R., Gascuel-Odoux, C., Gilliet, N., Grimaldi, C., & Gruau, G. (2015). Distinct export dynamics for dissolved and particulate phosphorus reveal independent transport mechanisms in an arable headwater catchment. *Hydrological Processes*, *29*(14), 3162–3178. https://doi.org/10.1002/hyp.10432

Dupas, R., Tittel, J., Jordan, P., Musolff, A., & Rode, M. (2018). Non-domestic phosphorus release in rivers during low-flow: Mechanisms and implications for sources identification. *Journal of Hydrology*, *560*, 141–149. https://doi.org/10.1016/j.jhydrol.2018.03.023

Elser, J. J., Peace, A. L., Kyle, M., Wojewodzic, M., McCrackin, M. L., Andersen, T., & Hessen, D. O. (2010). Atmospheric nitrogen deposition is associated with elevated phosphorus limitation of lake zooplankton. *Ecology Letters*, *13*(10), 1256–1261. https://doi.org/10.1111/j.1461-0248.2010.01519.x

Etheridge, J. R., Birgand, F., Osborne, J. A., Osburn, C. L., Michael, B. R., & Irving, J. (2014). Using in situ ultraviolet-visual spectroscopy to measure nitrogen, carbon, phosphorus, and suspended solids concentrations at a high frequency in a brackish tidal marsh. *Limnology and Oceanography Methods*, *12*(1), 10–22. https://doi.org/10.4319/lom.2014.12.10

Fitzhugh, R. D., Driscoll, C. T., Groffman, P. M., Tierney, G. L., Fahey, T. J., & Hardy, J. P. (2001). Effects of soil freezing disturbance on soil solution nitrogen, phosphorus, and carbon chemistry in a northern hardwood ecosystem. *Biogeochemistry*, *56*(2), 215–238. https://doi.org/10.1023/a:1013076609950

Fitzhugh, R. D., Likens, G. E., Driscoll, C. T., Mitchell, M. J., Groffman, P. M., Fahey, T. J., & Hardy, J. P. (2003). Role of soil freezing events in interannual patterns of stream chemistry at the Hubbard Brook experimental forest, New Hampshire. *Environmental Science & Technology*, *37*(8), 1575–1580. https://doi.org/10.1021/es026189r

Fovet, O., Humbert, G., Dupas, R., Gascuel-Odoux, C., Gruau, G., Jaffrezic, A., et al. (2018). Seasonal variability of stream water quality response to storm events captured using high-frequency and multi-parameter data. *Journal of Hydrology*, *559*, 282–293. https://doi.org/10.1016/j.jhydrol.2018.02.040

Frazar, S., Gold, A. J., Addy, K., Moatar, F., Birgand, F., Schroth, A. W., et al. (2019). Contrasting behavior of nitrate and phosphate flux from high flow events on small agricultural and urban watersheds. *Biogeochemistry*, *145*(1–2), 141–160. https://doi.org/10.1007/s10533-019-00596-z

Frost, P. C., Cross, W. F., & Benstead, J. P. (2005). Ecological stoichiometry in freshwater benthic ecosystems: An introduction. *Freshwater Biology*, *50*(11), 1781–1785. https://doi.org/10.1111/j.1365-2427.2005.01457.x

Frost, P. C., Kinsman, L. E., Johnston, C. A., & Larson, J. H. (2009). Watershed discharge modulates relationships between landscape components and nutrient ratios in stream seston. *Ecology*, *90*(6), 1631–1640. https://doi.org/10.1890/08-1534.1

Fuss, C. B., Driscoll, C. T., Groffman, P. M., Campbell, J. L., Christenson, L. M., Fahey, T. J., et al. (2016). Nitrate and dissolved organic carbon mobilization in response to soil freezing variability. *Biogeochemistry*, *131*(1), 35–47. https://doi.org/10.1007/s10533-016-0262-0

Gächter, R., Steingruber, S. M., Reinhardt, M., & Wehrli, B. (2004). Nutrient transfer from soil to surface waters: Differences between nitrate and phosphate. *Aquatic Sciences*, *66*(1), 117–122. https://doi.org/10.1007/s00027-003-0661-x

Gao, Y., Zhu, B., Yu, G., Chen, W., He, N., Wang, T., & Miao, C. (2014). Coupled effects of biogeochemical and hydrological processes on C, N, and P export during extreme rainfall events in a purple soil watershed in southwestern China. *Journal of Hydrology*, *511*(C), 692–702. https://doi.org/10.1016/j.jhydrol.2014.02.005

Goodale, C. L., Thomas, S. A., Fredriksen, G., Elliott, E. M., Flinn, K. M., Butler, T. J., & Walter, T. M. (2009). Unusual seasonal patterns and inferred processes of nitrogen retention in forested headwaters of the Upper Susquehanna River. *Biogeochemistry*, *93*(3), 197–218. https://doi.org/10.1007/s10533-009-9298-8

Goswami, S., Fisk, M. C., Vadeboncoeur, M. A., Garrison-Johnston, M., Yanai, R. D., & Fahey, T. J. (2018). Phosphorus limitation of aboveground production in northern hardwood forests. *Ecology*, *99*(2), 438–449. https://doi.org/10.1002/ecy.2100

Green, M. B., & Finlay, J. C. (2010). Patterns of hydrologic control over stream water total nitrogen to total phosphorus ratios. *Biogeochemistry*, *99*(1–3), 15–30. https://doi.org/10.1007/s10533-009-9394-9

Green, M. B., Nieber, J. L., Johnson, G., Magner, J., & Schaefer, B. (2007). Flow path influence on an N:P ratio in two headwater streams: A paired watershed study. *Journal of Geophysical Research*, *112*, G03015. https://doi.org/10.1029/2007JG000403

Green, M. B., & Wang, D. (2008). Watershed flow paths and stream water nitrogen-to-phosphorus ratios under simulated precipitation regimes. *Water Resources Research*, *44*, W12414. https://doi.org/10.1029/2007WR006139

Groffman, P. M., Cavender-Bares, J., Bettez, N. D., Grove, J. M., Hall, S. J., Heffernan, J. B., et al. (2014). Ecological homogenization of urban USA. *Frontiers in Ecology and the Environment*, *12*(1), 74–81. https://doi.org/10.1890/120374

Gu, S., Gruau, G., Dupas, R., Rumpel, C., Crème, A., Fovet, O., et al. (2017). Release of dissolved phosphorus from riparian wetlands: Evidence for complex interactions among hydroclimate variability, topography and soil properties. *Science of the Total Environment*, *598*(C), 421–431. https://doi.org/10.1016/j.scitotenv.2017.04.028

Guilbert, J., Betts, A. K., Rizzo, D. M., Beckage, B., & Bomblies, A. (2015). Characterization of increased persistence and intensity of precipitation in the northeastern United States. *Geophysical Research Letters*, *42*, 1888–1893. https://doi.org/10.1002/2015GL063124

Harrison, M. D., Groffman, P. M., Mayer, P. M., Kaushal, S. S., & Newcomer, T. A. (2011). Denitrification in alluvial wetlands in an urban landscape. *Journal of Environment Quality*, *40*(2), 634–646. https://doi.org/10.2134/jeq2010.0335

Hobara, S., Koba, K., Osono, T., Tokuchi, N., Ishida, A., & Kameda, K. (2005). Nitrogen and phosphorus enrichment and balance in forests colonized by comorants: Implications of the influence of soil adsorption. *Plant and Soil*, *268*(1), 89–101. https://doi.org/10.1007/s11104-004-0231-6

Hobbie, S. E., Finlay, J. C., Janke, B. D., Nidzgorski, D. A., Millet, D. B., & Baker, L. A. (2017). Contrasting nitrogen and phosphorus budgets in urban watersheds and implications for managing urban water pollution. *Proceedings of the National Academy of Sciences*, *114*, 4177–4182. https://doi.org/10.1073/pnas.1618536114

Hoffmann, C. C., Kjaergaard, C., Uusi-Kämppä, J., Hansen, H. C. B., & Kronvang, B. (2009). Phosphorus retention in riparian buffers: Review of their efficiency. *Journal of Environment Quality*, *38*(5), 1942–1955. https://doi.org/10.2134/jeq2008.0087

Holtan, H., Kamp-Nielsen, L., & Stuanes, A. O. (1988). Phosphorus in soil, water and sediment: An overview. *Hydrobiologia*, *170*(1), 19–34. https://doi.org/10.1007/BF00024896

Hrachowitz, M., Benettin, P., van Breukelen, B. M., Fovet, O., Howden, N. J. K., Ruiz, L., et al. (2016). Transit times-the link between hydrology and water quality at the catchment scale. *Wiley Interdisciplinary Reviews: Water*, *3*(5), 629–657. https://doi.org/10.1002/wat2.1155

Inamdar, S. P., O'Leary, N., Mitchell, M. J., & Riley, J. T. (2006). The impact of storm events on solute exports from a glaciated forested watershed in western New York, USA. *Hydrological Processes*, *20*(16), 3423–3439. https://doi.org/10.1002/hyp.6141

Isles, P. D., Xu, Y., Stockwell, J. D., & Schroth, A. W. (2017). Climate-driven changes in energy and mass inputs systematically alter nutrient concentration and stoichiometry in deep and shallow regions of Lake Champlain. *Biogeochemistry*, *133*(2), 201–217. https://doi.org/10.1007/s10533-017-0327-8

Janke, B. D., Finlay, J. C., Hobbie, S. E., Baker, L. A., Sterner, R. W., Nidzgorski, D., & Wilson, B. N. (2013). Contrasting influences of stormflow and baseflow pathways on nitrogen and phosphorus export from an urban watershed. *Biogeochemistry*, *121*(1), 209–228. https://doi.org/10.1007/s10533-013-9926-1

Jencso, K. G., McGlynn, B. L., Gooseff, M. N., Wondzell, S. M., Bencala, K. E., & Marshall, L. A. (2009). Hydrologic connectivity between landscapes and streams: Transferring reach- and plot-scale understanding to the catchment scale. *Water Resources Research*, *45*, W04428. https://doi.org/10.1029/2008WR007225

Jordan, S. J., Stoffer, J., & Nestlerode, J. A. (2011). Wetlands as sinks for reactive nitrogen at continental and global scales: A meta-analysis. *Ecosystems*, *14*(1), 144–155. https://doi.org/10.1007/s10021-010-9400-z

Judd, K. E., Likens, G. E., Buso, D. C., & Bailey, A. S. (2010). Minimal response in watershed nitrate export to severe soil frost raises questions about nutrient dynamics in the Hubbard Brook experimental forest. *Biogeochemistry*, *106*(3), 443–459. https://doi.org/10.1007/s10533-010-9524-4

Kaye, J. P., Groffman, P. M., Grimm, N. B., Baker, L. A., & Pouyat, R. V. (2006). A distinct urban biogeochemistry? *Trends in Ecology and Evolution*, *21*(4), 192–199. https://doi.org/10.1016/j.tree.2005.12.00

Kincaid, D. W., Seybold, E. C., Adair, E. C., Bowden, W. B., Perdrial, J. N., Vaughan, M. C. H., & Schroth, A. W. (2020). Vermont EPSCoR stream stations: 2014-2018 high-frequency discharge, nitrate, and SRP data. *HydroShare*. https://doi.org/10.4211/hs.85fa32a11fbb49779033934a135f54ef

Koenig, L. E., Shattuck, M. D., Snyder, L. E., Potter, J. D., & McDowell, W. H. (2017). Deconstructing the effects of flow on DOC, nitrate, and major ion interactions using a high-frequency aquatic sensor network. *Water Resources Research*, *53*, 10,655–10,673. https://doi.org/10.1002/2017WR020739

Langergraber, G., Fleischmann, N., & Hofstädter, F. (2003). A multivariate calibration procedure for UV/VIS spectrometric quantification of organic matter and nitrate in wastewater. *Water Science & Technology*, *47*(2), 63–71. https://doi.org/10.2166/wst.2003.0086

Lloyd, C. E. M., Freer, J. E., Johnes, P. J., & Collins, A. L. (2016). Technical note: Testing an improved index for analysing storm discharge-concentration hysteresis. *Hydrology and Earth System Sciences*, *20*(2), 625–632. https://doi.org/10.5194/hess-20-625-2016

McMillan, S. K., Wilson, H. F., Tague, C. L., Hanes, D. M., Inamdar, S., Karwan, D. L., et al. (2018). Before the storm: Antecedent conditions as regulators of hydrologic and biogeochemical response to extreme climate events. *Biogeochemistry*, *141*(3), 487–501. https://doi.org/10.1007/s10533-018-0482-6

Mevik, B.-H., Wehrens, R., & Liland, K. H. (2018). pls: Partial least squares and principal component regression. *R Package*.

Meyer, J. L., & Likens, G. E. (1979). Transport and transformation of phosphorus in a forest stream ecosystem. *Ecology*, *60*(6), 1255–1269. https://doi.org/10.2307/1936971

Michalak, A. M., Anderson, E. J., Beletsky, D., Boland, S., Bosch, N. S., Bridgeman, T. B., et al. (2013). Record-setting algal bloom in Lake Erie caused by agricultural and meteorological trends consistent with expected future conditions. *Proceedings of the National Academy of Sciences*, *110*(16), 6448–6452. https://doi.org/10.1073/pnas.1216006110

Mitchell, M. J., Driscoll, C. T., Kahl, J. S., Murdoch, P. S., & Pardo, L. H. (1996). Climatic control of nitrate loss from forested watersheds in the Northeast United States. *Environmental Science & Technology*, *30*(8), 2609–2612. https://doi.org/10.1021/es9600237

Moore, R. D. (2005). Introduction to salt dilution gauging for streamflow measurement Part III: Slug injection using salt in solution. *Streamline Watershed Management Bulletin*, *8*(2), 1–28.

Mulholland, P. J. (2004). The importance of in-stream uptake for regulating stream concentrations and outputs of N and P from a forested watershed: Evidence from long-term chemistry records for Walker Branch Watershed. *Biogeochemistry*, *70*(3), 403–426. https://doi.org/10.1007/s10533-004-0364-y

Nathan, R. J., & McMahon, T. A. (1990). Evaluation of automated techniques for base flow and recession analyses. *Water Resources Research*, *26*(7), 1465–1473. https://doi.org/10.1029/WR026i007p01465

Ockenden, M. C., Deasy, C. E., Benskin, C. M. H., Beven, K. J., Burke, S., Collins, A. L., et al. (2016). Changing climate and nutrient transfers: Evidence from high temporal resolution concentration-flow dynamics in headwater catchments. *Science of the Total Environment*, *548-549*(C), 325–339. https://doi.org/10.1016/j.scitotenv.2015.12.086

Oeurng, C., Sauvage, S., & Sánchez-Pérez, J.-M. (2010). Temporal variability of nitrate transport through hydrological response during flood events within a large agricultural catchment in south-west France. *Science of the Total Environment*, *409*(1), 140–149. https://doi.org/10.1016/j.scitotenv.2010.09.006

Outram, F. N., Cooper, R. J., Sünnenberg, G., Hiscock, K. M., & Lovett, A. A. (2016). Antecedent conditions, hydrological connectivity and anthropogenic inputs: Factors affecting nitrate and phosphorus transfers to agricultural headwater streams. *Science of the Total Environment*, *545–546*(1), 184–199. https://doi.org/10.1016/j.scitotenv.2015.12.025

Outram, F. N., Lloyd, C. E. M., Jonczyk, J., Benskin, C. M., Grant, F., Perks, M. T., et al. (2014). High-frequency monitoring of nitrogen and phosphorus response in three rural catchments to the end of the 2011–2012 drought in England. *Hydrology and Earth System Sciences*, *18*(9), 3429–3448. https://doi.org/10.5194/hess-18-3429-2014

Parsons, T. R., Maita, Y., & Lalli, C. M. (1984). Determination of phosphate. In T. R. Parsons, Y. Maita, C. M. Lalli (Eds.), *A manual of chemical and biological methods for seawater analysis* (pp. 22–25). Pergamon: Pergamon Press.

Paternoster, R., Brame, R., Mazerolle, P., & Piquero, A. (1998). Using the correct statistical test for the equality of regression coefficients. *Criminology*, *36*(4), 859–866. https://doi.org/10.1111/j.1745-9125.1998.tb01268.x

Pellerin, B. A., Saraceno, J. F., Shanley, J. B., Sebestyen, S. D., Aiken, G. R., Wollheim, W. M., & Bergamaschi, B. A. (2012). Taking the pulse of snowmelt: In situ sensors reveal seasonal, event and diurnal patterns of nitrate and dissolved organic matter variability in an upland forest stream. *Biogeochemistry*, *108*(1–3), 183–198. https://doi.org/10.1007/s10533-011-9589-8

Perdrial, J. N., McIntosh, J., Harpold, A., Brooks, P. D., Zapata-Rios, X., Ray, J., et al. (2014). Stream water carbon controls in seasonally snow-covered mountain catchments: Impact of inter-annual variability of water fluxes, catchment aspect and seasonal processes. *Biogeochemistry*, *118*(1–3), 273–290. https://doi.org/10.1007/s10533-013-9929-y

Piatek, K. B., Mitchell, M. J., Silva, S. R., & Kendall, C. (2005). Sources of nitrate in snowmelt discharge: Evidence from water chemistry and stable isotopes of nitrate. *Water Air and Soil Pollution*, *165*(1–4), 13–35. https://doi.org/10.1007/s11270-005-4641-8

Poor, C. J., & McDonnell, J. J. (2007). The effects of land use on stream nitrate dynamics. *Journal of Hydrology*, *332*(1–2), 54–68. https://doi.org/10.1016/j.jhydrol.2006.06.022

Poxleitner, M., Trommer, G., Lorenz, P., & Stibor, H. (2016). The effect of increased nitrogen load on phytoplankton in a phosphorus-limited lake. *Freshwater Biology*, *61*(11), 1966–1980. https://doi.org/10.1111/fwb.12829

Reckhow, K. H., Beaulac, M. N., & Simpson, J. T. (1980). Modeling phosphorus loading and lake response under uncertainty: A manual and compilation of export coefficients. Publication 440/5–80-011. United States Environmental Protection Agency.

Rose, L. A., Karwan, D. L., & Godsey, S. E. (2018). Concentration-discharge relationships describe solute and sediment mobilization, reaction, and transport at event and longer timescales. *Hydrological Processes*, *32*(18), 2829–2844. https://doi.org/10.1002/hyp.13235

Rosenberg, B. D., & Schroth, A. W. (2017). Coupling of reactive riverine phosphorus and iron species during hot transport moments: Impacts of land cover and seasonality. *Biogeochemistry*, *132*(1–2), 103. https://doi.org/10.1007/s10533-016-0290-9

Royer, T. V., David, M. B., & Gentry, L. E. (2006). Timing of riverine export of nitrate and phosphorus from agricultural watersheds in Illinois: Implications for reducing nutrient loading to the Mississippi River. *Environmental Science & Technology*, *40*(13), 4126–4131. https://doi.org/10.1021/es052573n

Sardans, J., Rivas-Ubach, A., & Peñuelas, J. (2011). The elemental stoichiometry of aquatic and terrestrial ecosystems and its relationships with organismic lifestyle and ecosystem structure and function: A review and perspectives. *Biogeochemistry*, *111*(1–3), 1–39. https://doi.org/10.1007/s10533-011-9640-9

Sebestyen, S. D., Boyer, E. W., Shanley, J. B., Kendall, C., Doctor, D. H., Aiken, G. R., & Ohte, N. (2008). Sources, transformations, and hydrological processes that control stream nitrate and dissolved organic matter concentrations during snowmelt in an upland forest. *Water Resources Research*, *44*, W12410. https://doi.org/10.1029/2008WR006983

Sebestyen, S. D., Shanley, J. B., Boyer, E. W., Kendall, C., & Doctor, D. H. (2014). Coupled hydrological and biogeochemical processes controlling variability of nitrogen species in streamflow during autumn in an upland forest. *Water Resources Research*, *50*, 1569–1591. https://doi.org/10.1002/2013WR013670

Seybold, E., Gold, A. J., Inamdar, S. P., Adair, C., Bowden, W. B., Vaughan, M. C. H., et al. (2019). Influence of land use and hydrologic variability on seasonal dissolved organic carbon and nitrate export: Insights from a multi-year regional analysis for the northeastern USA. *Biogeochemistry*, *146*(1), 31–49. https://doi.org/10.1007/s10533-019-00609-x

Sharpley, A. N., Kleinman, P. J., Heathwaite, A. L., Gburek, W. J., Folmar, G. J., & Schmidt, J. P. (2008). Phosphorus loss from an agricultural watershed as a function of storm size. *Journal of Environment Quality*, *37*(2), 362–368. https://doi.org/10.2134/jeq2007.0366

Siwek, J., Siwek, J. P., & Żelazny, M. (2012). Environmental and land use factors affecting phosphate hysteresis patterns of stream water during flood events (Carpathian Foothills, Poland). *Hydrological Processes*, *27*(25), 3674–3684. https://doi.org/10.1002/hyp.9484

Smith, V. H. (1983). Low nitrogen to phosphorus ratios favor dominance by blue-green algae in lake phytoplankton. *Science*, *221*(4611), 669–671. https://doi.org/10.1126/science.221.4611.669

Smith, V. H. (2006). Responses of estuarine and coastal marine phytoplankton to nitrogen and phosphorus enrichment. *Limnology and Oceanography*, *51*(1part2), 377–384. https://doi.org/10.4319/lo.2006.51.1_part_2.0377

Sobczak, W. V., Findlay, S., & Dye, S. (2003). Relationships between DOC bioavailability and nitrate removal in an upland stream: An experimental approach. *Biogeochemistry*, *62*(3), 309–327. https://doi.org/10.1023/a:1021192631423

Stieglitz, M., Shaman, J., McNamara, J., Engel, V., Shanley, J., & Kling, G. W. (2003). An approach to understanding hydrologic connectivity on the hillslope and the implications for nutrient transport. *Global Biogeochemical Cycles*, *17*(4), 1105. https://doi.org/10.1029/2003GB002041

Stutter, M. I., Langan, S. J., & Cooper, R. J. (2008). Spatial contributions of diffuse inputs and within-channel processes to the form of stream water phosphorus over storm events. *Journal of Hydrology*, *350*(3–4), 203–214. https://doi.org/10.1016/j.jhydrol.2007.10.045

Surridge, B. W. J., Heathwaite, A. L., & Baird, A. J. (2007). The release of phosphorus to porewater and surface water from river riparian sediments. *Journal of Environment Quality*, *36*(5), 1534–1544. https://doi.org/10.2134/jeq2006.0490

Taguchi, V. J., Olsen, T. A., Natarajan, P., Janke, B. D., Gulliver, J. S., Finlay, J. C., & Stefan, H. G. (2020). Internal loading in stormwater ponds as a phosphorus source to downstream waters. *Limnology and Oceanography Letters*. Advance online publication, *5*(4), 322–330. https://doi.org/10.1002/lol2.10155

Tang, W., & Carey, S. K. (2017). HydRun: A MATLAB toolbox for rainfall-runoff analysis. *Hydrological Processes*, *31*(15), 2670–2682. https://doi.org/10.1002/hyp.11185

Tilman, D., Kilham, S. S., & Kilham, P. (1982). Phytoplankton community ecology: The role of limiting nutrients. *Annual Review of Ecology and Systematics*, *13*(1), 349–372. https://doi.org/10.1146/annurev.es.13.110182.002025

Turner, B. L., & Haygarth, P. M. (2001). Phosphorus solubilization in rewetted soils. *Nature*, *411*(6835), 258–258. https://doi.org/10.1038/35077146

Turnipseed, D. P., & Sauer, V. B. (2010). Discharge measurements at gaging stations. In *U.S. Geological Survey Techniques and Methods, Book 3*. Reston, VA: U.S. Geological Survey.

Underwood, K. L., Rizzo, D. M., Schroth, A. W., & Dewoolkar, M. M. (2017). Evaluating spatial variability in sediment and phosphorus concentration-discharge relationships using Bayesian inference and self-organizing maps. *Water Resources Research*, *53*, 10,293–10,316. https://doi.org/10.1002/2017WR021353

van Herpe, V. Y., & Troch, P. A. (2000). Spatial and temporal variations in surface water nitrate concentrations in a mixed land use catchment under humid temperate climatic conditions. *Hydrological Processes*, *14*(14), 2439–2455. https://doi.org/10.1002/1099-1085(20001015)14:14<2439::aid-hyp105>3.0.co;2-h

Vanni, M. J., Renwick, W. H., Headworth, J. L., Auch, J. D., & Schaus, M. H. (2001). Dissolved and particulate nutrient flux from three adjacent agricultural watersheds: A five-year study. *Biogeochemistry*, *54*(1), 85–114. https://doi.org/10.1023/a:1010681229460

Vaughan, M. C. H., Bowden, W. B., Shanley, J. B., Vermilyea, A., & Schroth, A. W. (2019). Shining light on the storm: In-stream optics reveal hysteresis of dissolved organic matter character. *Biogeochemistry*, *143*(3), 275–291. https://doi.org/10.1007/s10533-019-00561-w

Vaughan, M. C. H., Bowden, W. B., Shanley, J. B., Vermilyea, A., Sleeper, R., Gold, A. J., et al. (2017). High-frequency dissolved organic carbon and nitrate measurements reveal differences in storm hysteresis and loading in relation to land cover and seasonality. *Water Resources Research*, *53*, 5345–5363. https://doi.org/10.1002/2017WR020491

Vaughan, M. C. H., Bowden, W. B., Shanley, J. B., Vermilyea, A., Wemple, B., & Schroth, A. W. (2018). Using in situ UV-visible spectrophotometer sensors to quantify riverine phosphorus partitioning and concentration at a high frequency. *Limnology and Oceanography Methods*, *16*, 840–855. https://doi.org/10.1002/lom3.10287

Watmough, S. A., Eimers, M. C., Aherne, J., & Dillon, P. J. (2004). Climate effects on stream nitrate concentrations at 16 forested catchments in south central Ontario. *Environmental Science & Technology*, *38*(8), 2383–2388. https://doi.org/10.1021/es035126l

Webster, J. R., Newbold, J. D., Thomas, S. A., Valett, H. M., & Mulholland, P. J. (2009). Nutrient uptake and mineralization during leaf decay in streams—A model simulation. *International Review of Hydrobiology*, *94*(4), 372–390. https://doi.org/10.1002/iroh.200811158